LETTERS

Giant aeolian dune size determined by the average depth of the atmospheric boundary layer

Bruno Andreotti[1], Antoine Fourrière[1], Fouzia Ould-Kaddour[2], Brad Murray[3] & Philippe Claudin[1]

Depending on the wind regime[1,2], sand dunes exhibit linear[3,4], crescent-shaped or star-like forms[5] resulting from the interaction between dune morphology and sand transport[6–8]. Small-scale dunes form by destabilization of the sand bed[9–11] with a wavelength (a few tens of metres) determined by the sand transport saturation length[11–13]. The mechanisms controlling the formation of giant dunes, and in particular accounting for their typical time and length scales, have remained unknown. Using a combination of field measurements and aerodynamic calculations, we show here that the growth of aeolian giant dunes, ascribed to the nonlinear interaction between small-scale superimposed dunes[4,10,14,15], is limited by the confinement of the flow within the atmospheric boundary layer[16,17]. Aeolian giant dunes and river dunes form by similar processes, with the thermal inversion layer that caps the convective boundary layer in the atmosphere[18] acting analogously to the water surface in rivers. In both cases, the bed topography excites surface waves on the interface that in turn modify the near-bed flow velocity. This mechanism is a stabilizing process that prevents the scale of the pattern from coarsening beyond the resonant condition. Our results can explain the mean spacing of aeolian giant dunes ranging from 300 m in coastal terrestrial deserts to 3.5 km. We propose that our findings could serve as a starting point for the modelling of long-term evolution of desert landscapes under specific wind regimes.

Aeolian dune fields generically present two well-separated length scales[15,19,20] (Fig. 1). The smallest superimposed bed-forms have been explained by a linear aerodynamic instability the initial wavelength λ_s of which is related to the length needed for sand transport to reach equilibrium with the wind strength[11–13] and are thus called 'elementary dunes'. Tentative explanations for the formation of giant dunes have proposed specific dynamics associated with the different types of dunes, thought of as isolated objects[4,5]. In contrast, we hypothesize that the emergence of giant transverse, longitudinal and star dunes results from collective processes, the symmetries of the different patterns resulting from those of the wind rose. Indeed, both small- and large-scale dunes share the same symmetries under a common wind regime (Fig. 1). Furthermore, the different types of giant dunes exhibit the same characteristic wavelength λ_g, of the order of a kilometre (Fig. 1), and feature superimposed structures the avalanche slip faces of which show separations on the same scale λ_s. These commonalities suggest that the key dynamical processes forming giant dunes are not to be looked for in the shape of the pattern but in the understanding of the characteristic time and length scales resulting from their formation. We propose a novel collective mechanism in which the average structure of the atmosphere determines the giant scale.

The dryness of deserts results primarily from the overall stability of the atmosphere in anticyclonic regions. The stable stratification of the free atmosphere, characterized by the Brunt-Väisälä frequency $N = \sqrt{\frac{g}{\theta}\frac{d\theta}{dz}}$ (where g is the gravity and θ is the virtual potential temperature) for restoring vertically displaced air parcels, prevents the development of turbulence. The temperature gradient $\gamma = d\theta/dz \approx 4 \, \text{K km}^{-1}$ is largely independent of the location and the season (Supplementary Information 1). In winter, the heat flux from the surface is insufficient to produce convection, so the atmospheric boundary layer is stably stratified almost down to the ground (Fig. 2b). In warmer seasons, however, a convective (well-mixed) boundary layer forms, in which the temperature and the horizontal wind velocity are roughly homogeneous. A thermal inversion (capping) layer, characterized by a jump in air density $\Delta\rho$ separates stable and unstable layers. The shear stress τ decreases linearly with height in the well-mixed layer, vanishes at the capping altitude H and remains null in the free atmosphere[18]. The base flow is thus similar to that in a river. Furthermore, gravity waves can propagate at a speed c on this atmospheric interface, as they do along the free surface of a river[21]. Introducing the wavenumber $k = 2\pi/\lambda$, the surface-wave dispersion relation can be approximated by:

$$c^2 + \left(1 - \frac{\Delta\rho}{\rho_0}\right) c \sqrt{c^2 - \frac{N^2}{k^2}} = \frac{\Delta\rho}{\rho_0}\frac{g}{k} \qquad (1)$$

in the limit of large kH. The river case is recovered for $\Delta\rho \approx \rho_0$ and $N = 0$. Consequently, aeolian giant dune relief can excite standing surface waves that in turn modify the wind speed and thus the sand transport.

Because the temperature profile $\theta(z)$ in the free atmosphere does not depend much on the season, the typical height of the capping layer H increases linearly with the ground temperature annual variations: $H \approx \delta\theta/\gamma$ (Fig. 2b). The ground temperature is controlled by thermal transfers at the synoptic scale and varies annually from a few degrees in temperate environments close to the seashore to a few tens of degrees in more continental regions (Supplementary Information 1). We expect modern temperature measurements to be relevant over the current Holocene interglacial. We have measured the giant dune wavelength λ in all homogeneous desert regions of the world (Supplementary Information 2) and shown that it is linearly correlated with $\delta\theta/\gamma$, independent of the dune symmetry (Fig. 2a). These data then strongly support the idea that the size of giant dunes scales with the depth of the atmospheric boundary layer.

To understand the origin of this relation, we have computed the two-dimensional turbulent flow confined between a capping stratified fluid and a wavy bottom (Supplementary Information 7). Navier-Stokes equations are closed by the means of a Prandtl mixing length approach, and are expanded with respect to the bottom corrugation aspect ratio a/λ, which is a small parameter. A key output of these calculations is the phase shift between the bottom topography and the

[1]Laboratoire de Physique et Mécanique des Milieux Hétérogènes (PMMH UMR 7636 CNRS-ESPCI-P6-P7), 10 rue Vauquelin, 75005 Paris, France. [2]Laboratoire de Physique Théorique, Université Abou Bekr Belkaïd, Tlemcen, Algeria. [3]Nicholas School of the Environment and Earth Sciences, Center for Nonlinear and Complex Systems, Duke University, Box 90230, Durham, North Carolina 27708-0230, USA.
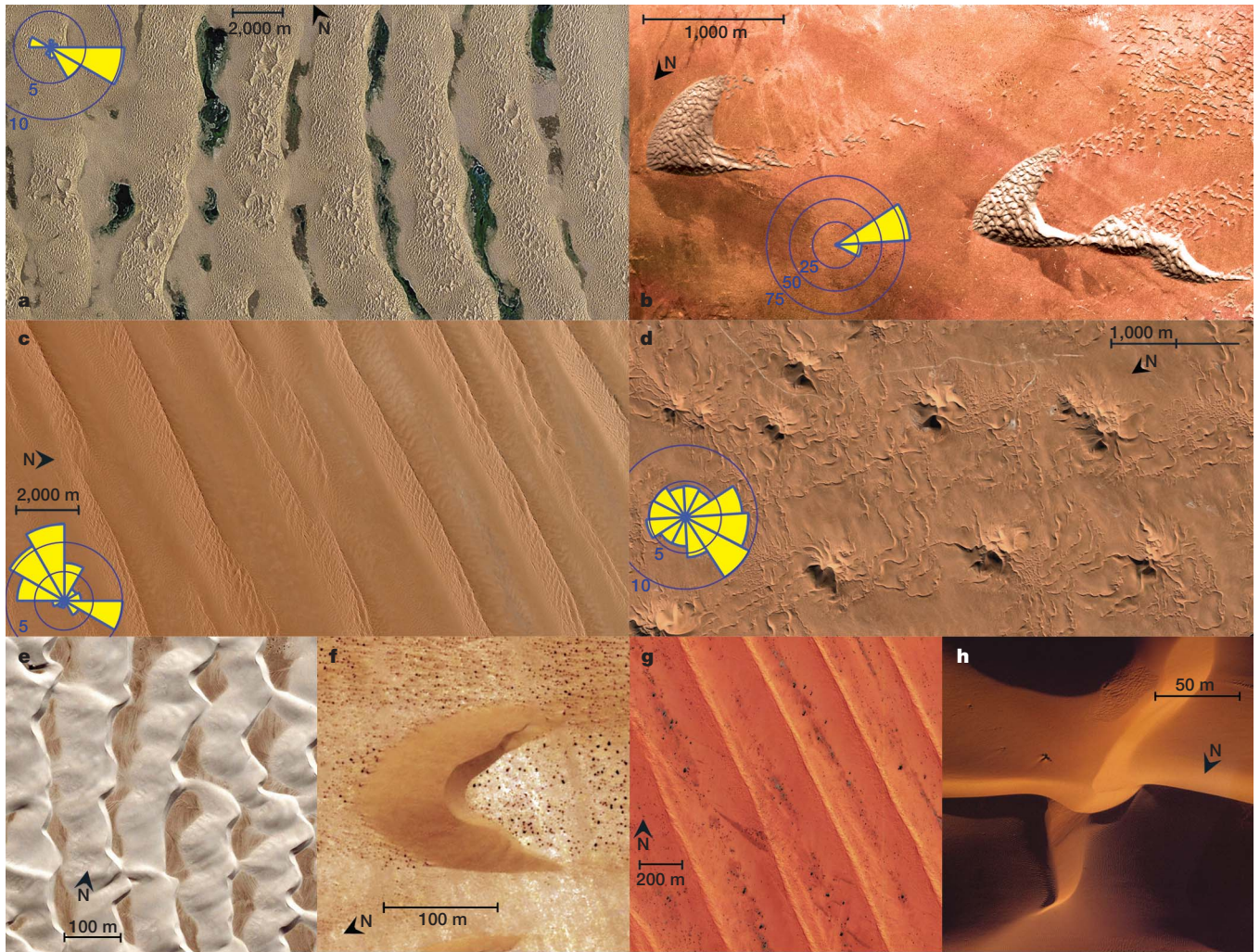
Figure 1 | Separation of length scales between small and giant dunes for the different wind regimes. a–d, Giant dunes. **a,** Transverse dunes, Badain Jaran (China, 38° 38′ N/104° 59′ E); **b,** crescent-shaped barchan, Atlantic Sahara (Morocco, 28° 02′ N/12° 11′ E); **c,** longitudinal dunes, RubAlKhali, (South Arabia, 18° 11′ N/47° 21′ E); **d,** star dunes, Grand Erg Oriental (Algeria, 31° 27′ N/07° 45′ E). **e–h,** Small dunes. **e,** White sands (USA, 32° 49′ N/106° 16′ W); **f,** Atlantic Sahara (Morocco, 27° 11′ N/13° 13′ W); **g,** Australia (23° 51′ S/136° 33′ E); **h,** Mauritania (18° 09′ N/15° 29′ W). These aerial photographs (credits: Digital Globe) show that giant dunes are not isolated objects but involve a composite spatial organization. The wind regimes are characterized by the averaged sand flux roses (1999–2007), on which yellow arrows indicate the direction in which the dominant wind moves. The symmetries of these roses are consistent with those of the giant dune pattern (Supplementary Information 5).
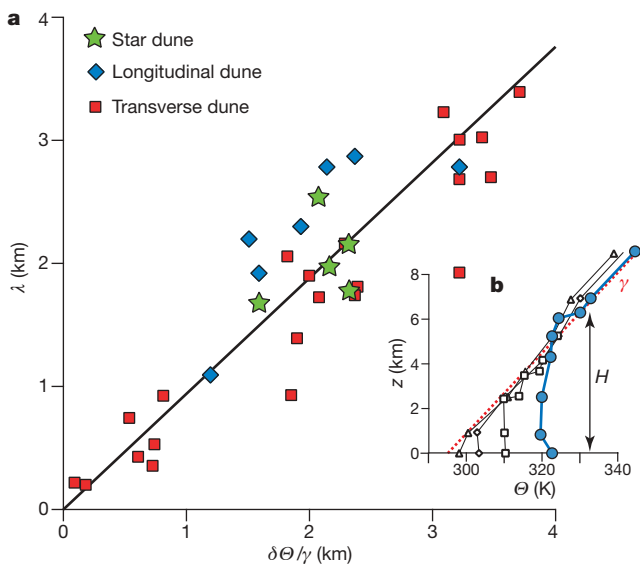
basal shear stress τ_b, which controls the linear growth of dunes[9–11]. Figure 3 shows that the fastest-growing wavelength always corresponds to elementary dunes ($\lambda = \lambda_s$). Furthermore, the presence of


Figure 2 | Selection of the wavelength of giant dunes by the depth of the atmospheric boundary layer. a, Measured giant dune wavelength λ as a function of the characteristic mixing height, computed from the annual ground temperature variations $\delta\theta$ (Supplementary Table). The solid line is the identity: $\lambda = \delta\theta/\gamma$. λ in some cases is the average dune spacing and in others is the peak wavelength in a Fourier spectrum (Supplementary Information 2). As the dune patterns present dislocation defects, the distribution of dune spacing must have a width of the order of λ. $\delta\theta$ is averaged over the period 2000–2007 (Supplementary Information 1). $\delta\theta$ mostly reflects the distance to the ocean, and is therefore likely to remain approximately constant at any location over the timescale of formation of giant dunes. **b,** Virtual potential temperature profiles $\theta(z)$, measured by sounding balloons at noon, in Sulayel (South Arabia, 20° 47′ N/45° 67′ E), at different seasons (blue circles: 27/07/1978, squares: 22/10/1978, diamonds: 01/12/1977, triangles: 12/02/1978). The free atmosphere preserves an almost steady linear profile (red dashed line) of slope $\gamma = 4\,\mathrm{K\,km^{-1}}$. The summer profile shows a 6-km-deep mixed layer. The winter profile is stably stratified nearly down to the soil. The residual mixing height ($<100\,\mathrm{m}$) is the altitude at which the mechanically produced turbulence is in balance with the dissipative effect of negative buoyancy.

the capping layer has an overall stabilizing effect, which is particularly pronounced at the scale H. When the fluid flows at the velocity U over a relief of wavelength λ, waves on the capping layer are generated at this wavelength. The system is resonant when U equals the wave propagation speed c at the wavenumber k. This situation corresponds to a shift of the maximum basal shear stress to downwind of the crest (Fig. 3), and thus to a stable situation in which bed perturbations decay[9–11]. With a free surface, the growth rate σ for wavelengths of the order of H is lower than it would be without a free surface (Fig. 3). Thus, the formation of giant dunes cannot be explained by a primary linear instability, that is, by a new growth-rate peak caused by the free surface.

To go beyond linear aerodynamics, we have extended the expansion of the flow field up to the third order in the aspect ratio a/λ, to get the first nonlinear corrections to the basal shear stress (Supplementary Information 7). The phase shift with respect to the bed eventually vanishes for some amplitude, which can be interpreted as the equilibrium height of a mature dune of a certain wavelength. For small λ, the selected aspect ratio is roughly constant ($a/\lambda \approx 1/12$) and matches quantitative observations[22,23] (Fig. 4c). For larger wavelengths, the presence of the capping layer causes dunes to stabilize at smaller aspect ratios (Fig. 4c). The resulting relation between the steady amplitude a and the wavelength λ presents a pronounced maximum, not very
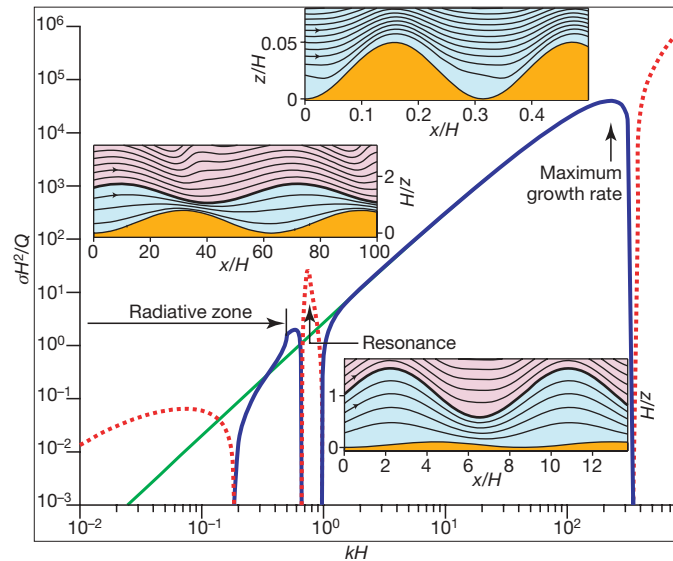
Figure 3 | Linear stability analysis of the dune formation process. Growth rate modulus $|\sigma|$ rescaled by the timescale H^2/Q (Q is the reference saturated sand flux[10]; H^2/Q ranges from 2,500 years in the Atlantic Sahara to 250,000 years in RubAlKhali) as a function of the rescaled wavenumber kH. Stable wavelengths ($\sigma < 0$) are shown by a dotted red line and unstable ones ($\sigma > 0$) are shown by a solid blue line. The curve obtained in the absence of a capping layer (in the limit of infinite H) is shown in green. Insets show streamlines over sinusoidal dunes (orange) computed at the linear order. The stratification of the free atmosphere (purple) is characterized by the non-dimensional number $B = U/HN = 2$, and the density discontinuity across the capping layer (bold line) that separates the well-mixed layer (blue) from the free atmosphere by $S = \rho_0 U^2/\Delta\rho gH = 0.7$. The Reynolds number is $Re = U\lambda/v = 10^8$. The wind blows from left to right (shown by arrows). The area where near-bed streamlines are most dense corresponds to the maximum shear stress, which separates an erosion zone upstream from a zone of accretion. Thus, if the maximum occurs upstream of the crest of a bed perturbation, the bump grows, and vice versa. The growth rate of small wavelength ($\lambda \ll H$) scales as Qk^2 and is maximum at λ_s. Accordingly, the streamlines are squeezed upstream of the dune crest (top inset, computed for $kH = 20$). At the surface wave resonance, for $U = c(k)$, the capping layer deforms such that the streamlines are squeezed downstream of the relief crest (bottom inset, computed for $kH = 0.7$). Beyond the radiative threshold, for $Uk < N$, standing internal waves are generated in the free atmosphere, which leads to the same stabilizing effect (left inset, computed for $kH = 0.1$).
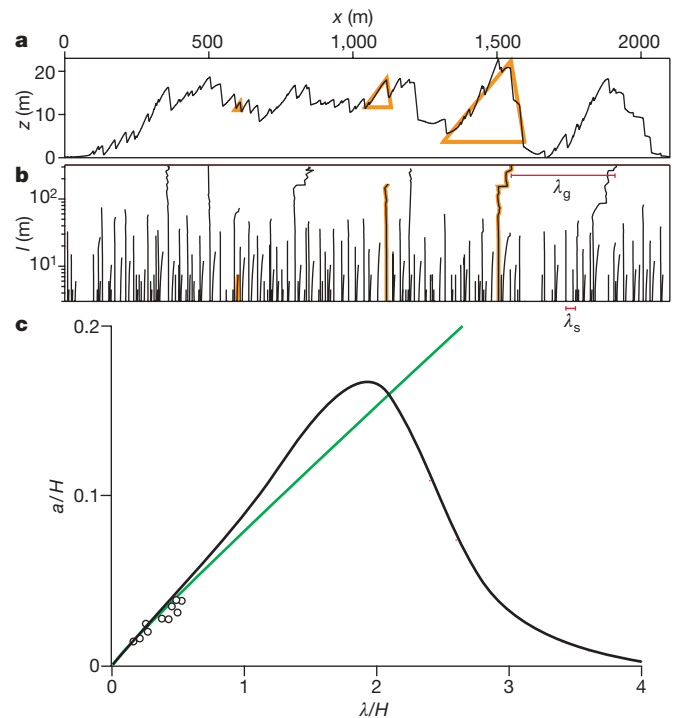
Figure 4 | Pattern coarsening and nonlinear wavelength selection.
a, Profile of transverse giant dunes in the Atlantic Sahara (28° 03′ N/12° 12′ W). The combination of GPS data and direct geometrical measurements (lengths, heights and angles) ensures an excellent relative and absolute accuracy. Nascent superimposed dunes are detected down to centimetre-scale amplitudes. **b**, Wavelet transform maxima represented in a scale-space diagram. In this multi-scale decomposition, each vertical line indicates the presence of a triangle-like sub-structure (see orange ones for example), whose length and position are given by the upper tip coordinates. **c**, Amplitude a of steady dunes as a function of their wavelength λ (both rescaled by H), predicted by the nonlinear aerodynamic model with a capping layer (black line, $B = U/HN = 0.7$, $S = \rho_0 U^2/\Delta\rho gH = 0.7$ and $Re = U\lambda/v = 10^8$) and without a capping layer (green line). Circles correspond to field data[22,23]. Confining the flow below the capping layer tends to compress streamlines over dune crests, reducing the steady amplitude (compared to the case without the capping layer) as wavelength increases from small values. Free-surface-wave effects then cause steady amplitudes to approach zero as wavelengths increase further.

sensitive to variations in parameters (Fig. 4c), and which corresponds to giant dunes commensurate with H.

As is supported by Ground Penetrating Radar studies of Pleistocene giant dunes[14], giant dunes are likely to result from the amalgamation[15] of superimposed dunes. Such progressive growth, ultimately limited by the average depth of the atmospheric boundary layer, sounds paradoxical in view of the separation between the scales of elementary dunes and giant dunes. Here we perform a wavelet analysis of field-measured giant dune profiles (Fig. 4a, b), which allows a determination of the length scales of the structures that compose these dunes, taking into account the whole relief and not only the horizontal succession of slip-faces. This analysis shows the large-scale modulation of the relief at the wavelength λ_g as well as the covering of elementary dunes at λ_s. It also reveals the presence of superimposed structures at all scales in between. This confirms that superimposed dunes grow progressively by merging, which is possible because the propagation velocity of superimposed bed-forms decreases with their size[10]. Elementary dunes are continuously regenerated because any sufficiently long flat sand area destabilizes linearly at the scale λ_s (ref. 10). Amalgamation results in a global pattern coarsening that follows the amplitude-wavelength curve of Fig. 4c. As the wavelength becomes comparable to the average atmospheric boundary layer depth, dune height is maximized, and the corresponding structures

dominate the atmospheric dynamics as well as the emergence of the pattern. The nonlinear selection of the maximum of the curve $a(\lambda)$ is a generic result of systems whose pattern coarsening results from a screening interaction between neighbouring objects[24] or from a phase-negative diffusion instability[25].

So far, the dynamical mechanisms involved—turbulence, resonant surface waves and dune interaction—are valid for subaqueous dunes[26,27] as well as aeolian ones. In the aeolian case, however, an additional stabilizing mechanism becomes important at small k that is not present in rivers (Fig. 3). It is related to the possibility of radiating internal waves into the atmosphere when the exciting frequency Uk is lower than N. In the subaqueous case this mechanism is not relevant, so that dunes with wavelengths much greater than the flow depth may grow. And indeed, very long river dunes, with wavelengths up to several tens of times the water depth, have been observed in large rivers[26]. We expect their formation mechanism to be of the same nature as for aeolian giant dunes. As on Earth, the atmospheric boundary layers on Mars and Titan[28,29] have kilometre-scale depths. However, the elementary wavelength on Mars is around 600 m (ref. 11), whereas on Titan it is expected to be of the order of a few metres; so although aeolian structures on Mars and Titan are comparable in size[30], only Titan's are giant dunes.

In this exploratory model, we have intentionally omitted several aspects needed to reproduce natural giant dunes in detail: three-dimensional shapes, the Coriolis effect, daily and seasonal atmospheric cycles, erratic winds. The good agreement with wavelength measurements indicates that the stabilizing influence of the free atmosphere is essential to our understanding of the emergence of all giant dune types.

1. Fryberger, S. G. & Dean, G. in *A Study of Global Sand Seas* (ed. McKee, E. D.) 137–169 (Geological Survey Professional Paper 1052, 1979).
2. Werner, B. T. Eolian dunes; computer simulations and attractor interpretation. *Geology* 23, 1107–1110 (1995).
3. Tsoar, H. Dynamic processes acting on a longitudinal (seif) sand dune. *Sedimentology* 30, 567–578 (1983).
4. Bristow, C. S., Bailey, S. D. & Lancaster, N. The sedimentary structure of linear sand dunes. *Nature* 406, 56–59 (2000).
5. Lancaster, N. The dynamics of star dunes: an example from Gran Desierto, Mexico. *Sedimentology* 36, 273–289 (1989).
6. Andreotti, B., Claudin, P. & Douady, S. Selection of dune shapes and velocities. Part 1: Dynamics of sand, wind and barchans. *Eur. Phys. J. B* 28, 321–339 (2002).
7. Wiggs, G. F. S., Livingstone, I. & Warren, A. The role of streamline curvature in sand dune dynamics: evidence from field and wind tunnel measurements. *Geomorphology* 17, 29–46 (1996).
8. Lancaster, N., Nickling, W. G., McKenna-Neuman, C. K. & Wyatt, V. E. Sediment flux and airflow on the stoss slope of a barchan dune. *Geomorphology* 17, 55–62 (1996).
9. Andreotti, B., Claudin, P. & Douady, S. Selection of dune shapes and velocities. Part 2. *Eur. Phys. J. B* 28, 341–352 (2002).
10. Elbelrhiti, H., Claudin, P. & Andreotti, B. Field evidence for surface-wave-induced instability of sand dunes. *Nature* 437, 720–723 (2005).
11. Claudin, P. & Andreotti, B. A scaling law for aeolian dunes on Mars, Venus, Earth, and for subaqueous ripples. *Earth Planet. Sci. Lett.* 252, 30–44 (2006).
12. Kroy, K., Sauermann, G. & Herrmann, H. Minimal model for sand dunes. *Phys. Rev. Lett.* 88, 054301 (2002).
13. Hersen, P., Douady, S. & Andreotti, B. Relevant length scale of barchan dunes. *Phys. Rev. Lett.* 89, 264301 (2002).
14. Bristow, C. S., Duller, G. A. T. & Lancaster, N. Age and dynamics of linear dunes in the Namib desert. *Geology* 35, 555–558 (2007).
15. Kocurek, G., Havholm, K. G., Deynoux, M. & Blakey, R. C. Amalgamated accumulations resulting from climatic and eustatic changes, Akchar Erg, Mauritania. *Sedimentology* 38, 751–772 (1991).
16. Wilson, I. G. Aeolian bedforms—their development and origins. *Sedimentology* 19, 173–210 (1972).
17. Hanna, S. R. The formation of longitudinal sand dunes by large helical eddies in the atmosphere. *J. Appl. Meteorol.* 8, 874–883 (1969).
18. Stull, R. B. *An Introduction to Boundary Layer Meteorology* Ch. 1, 11 (Kluwer Academic, 1988).
19. Lancaster, N. The development of large aeolian bedforms. *Sedim. Geol.* 55, 69–89 (1988).
20. Ewing, R. C., Kocurek, G. & Lake, L. W. Pattern analysis of dune-field parameters. *Earth Surf. Processes Landforms* 31, 1176–1191 (2006).
21. Wurtele, M. G., Sharman, R. D. & Datta, A. Atmospheric lee waves. *Annu. Rev. Fluid Mech.* 28, 429–476 (1996).
22. Baddock, M. C., Livingstone, I. & Wiggs, G. F. S. The geomorphological significance of airflow patterns in transverse dune interdunes. *Geomorphology* 87, 322–336 (2007).
23. Parteli, E. J. R., Schwämmle, V., Herrmann, H. J., Monteiro, L. H. U. & Maia, L. P. Profile measurement and simulation of a transverse dune field in the Lençóis Maranhenses. *Geomorphology* 81, 29–42 (2006).
24. Andersen, K. H., Chabanol, M.-L. & van Hecke, M. Dynamical models for sand ripples beneath surface waves. *Phys. Rev. E* 63, 066308 (2001).
25. Politi, P. & Misbah, C. When does coarsening occur in the dynamics of one-dimensional fronts? *Phys. Rev. Lett.* 92, 090601 (2004).
26. Best, J. The fluid dynamics of river dunes: a review and some future directions. *J. Geophys. Res.* 100, F04S02 (2005).
27. Raudkivi, A. J. Transition from ripples to dunes. *J. Hydraul. Eng.* 132, 1316–1320 (2006).
28. Tokano, T., Ferri, F., Colombatti, G., Mäkinen, T. & Fulchignoni, M. Titan's planetary boundary layer structure at the Huygens landing site. *J. Geophys. Res.* 111, E08007 (2006).
29. Savijärvi, H., Määttänen, A., Kauhanen, J. & Harri, A. M. Mars Pathfinder: New data and new model simulations. *Q. J. R. Meteorol. Soc.* 130, 669–683 (2004).
30. Lorenz, R. D. *et al.* The sand seas of Titan: Cassini RADAR observations of longitudinal dunes. *Science* 312, 724–727 (2006).